Aerospace Science and Technology 93 (2019) 105335

Contents lists available at ScienceDirect

Aerospace Science and Technology

www.elsevier.com/locate/aescte

A method to select loss correlations for centrifugal compressor performance prediction

Zhang Chaowei [a,b], Dong Xuezhi [a,b,*], Liu Xiyang [a,b], Sun Zhigang [a], Wu Shixun [a], Gao Qing [a,b], Tan Chunqing [a,b]

[a] Institute of Engineering Thermophysics, Chinese Academy of Sciences, Beijing 100190, PR China
[b] University of Chinese Academy of Sciences, Beijing 100049, PR China

ARTICLE INFO

Article history:
Received 20 May 2019
Received in revised form 27 July 2019
Accepted 9 August 2019
Available online 13 August 2019

Keywords:
Centrifugal compressor
Loss correlation set
Performance prediction
Specific speed
Inlet tip relative Mach number

ABSTRACT

The study reviews the main loss mechanisms and corresponding loss correlations, which are used to predict centrifugal compressor performance. There are one or more loss correlations in the open literature for the same loss mechanism. The purpose of this review is to identify a reliable loss correlation set for centrifugal compressor performance prediction. According to the inlet tip relative Mach number and specific speed, a new method to select loss correlations is proposed by testing multiple loss correlations. This method is validated by experimental results on eight centrifugal compressors in public and one in-house. The performance as-predicted by the proposed method is in close agreement with the experimental results. Compared with the conventional set, the proposed method is superior.

1. Introduction

Preliminary performance prediction is a crucial aspect of any effective centrifugal compressor design. Unknown parameters in the 1D performance prediction process such as slip factor and losses are dependent on empirical correlations or assumptions. Of these parameters, loss correlations play a particularly important role in predicting the centrifugal compressor performance. Previously published studies describe internal and parasitic losses in the impeller; in addition to these losses, enthalpy loss occurs in the inlet guide vane, vaneless diffuser and vaned diffuser. The literature describes one or more loss correlations for the same loss mechanism. To secure the sufficient accuracy to predict centrifugal compressor performance, it is necessary to find a reliable loss correlation set.

Several loss correlation sets have been proposed in recent years. Galvas [1], for example, proposed a 1D model to predict the performance of a centrifugal compressor with channel diffusers under off-design conditions. Unfortunately, the model has altogether insufficient accuracy. Conrad et al. [2] proposed a vaneless diffuser centrifugal compressor model to investigate all impeller losses in details. Whitfield and Baines [3] reviewed loss correlations in the open literature and introduced a general turbocharger centrifugal compressor model for performance prediction, where stage total pressure ratio reaches 2.4. Oh [4] presented an optimum loss correlation set to predict centrifugal compressor performance by testing most available internal and parasitic loss correlations. The set underestimates enthalpy loss in the low flow region, and the stage pressure ratio is only up to 2.1.

There have been many other important contributions to the literature. Gravdahl et al. [5] developed a model based on dynamic behavior of a compressor with the stage pressure ratio up to 1.4, but they only considered friction loss, incidence loss, mixing loss and blade loading. Doustmohammadi et al. [6] determined an optimum combination of loss correlations for a centrifugal compressor with a volute and stage pressure ratio up to 1.8. Li et al. [7] established a new set of loss correlation combinations by reviewing existing 1D loss correlations which contained loss correlations of the impeller, vaneless diffuser and vaned diffuser. Theirs outperformed Galvas's and Oh's loss correlation sets. However, at off-design speeds, especially at low speeds, there is large difference between the 1D calculation results and experimental data. Elkin [8] also found a suitable loss correlation set to predict performance under the design condition by testing most loss correlations, but it doesn't function well under off-design conditions.

The loss correlation sets discussed above don't include shock loss and can only be applied to lowly-loaded centrifugal com-

* Corresponding author at: Institute of Engineering Thermophysics, Chinese Academy of Sciences, Beijing 100190, PR China.
E-mail address: dongxuezhi@iet.cn (X. Dong).

https://doi.org/10.1016/j.ast.2019.105335
1270-9638/

Nomenclature

List of symbols

A	Flow area
AR	Area ratio
B	Aerodynamic blockage
b	Impeller width
b^*	The ratio of the vaneless diffuser inlet width to the impeller exit width
C_f	Skin friction coefficient
C_p	Specific heat at constant pressure
c	Clearance size
D	Diameter
DR	Diffusion ratio
D_{eq}	Equivalent diffusion factor
D_f	Diffusion factor
D_{hyd}	Impeller average hydraulic diameter
f_{inc}	Incidence coefficient
f_{df}	Skin friction coefficient
h	Static enthalpy
L_b	Impeller flow length
L_θ	Impeller meridional length
L_z	Impeller axial length
M	Mach number
m	Mass flow rate
n	Rotational speed
n_s	Specific speed
p	Static pressure
PR	Pressure ratio
Q	Volume flow rate
R_g	Gas constant of air
Re	Reynolds number
RMSE	Root-mean-square error
r	Radius
T	Static temperature
t	Blade thickness
U	Impeller periphery velocity
V	Absolute flow velocity
V_4^*	The absolute velocity at the optimum incidence angle
W	Relative flow velocity
Z	Number of blades
ΔH	Enthalpy change

Greek symbols

α	Absolute flow angle from meridional
β	Relative flow angle from meridional
ε_{wake}	Wake width
η	Isentropic efficiency
ν	Kinematic viscosity
μ	Slip factor
ρ	Density
γ	Specific heat ratio
χ	Wake mass fraction

Subscripts

0	Stagnation condition; Guide vane inlet
1	Guide vane outlet
2	Impeller inlet
3	Impeller outlet
4	Radial vaned diffuser inlet
5	Radial vaned diffuser outlet
6	Axial vaned diffuser inlet
7	Axial vaned diffuser outlet
avd	Axial vaned diffuser
b	Blade parameter
bl	Blade loading
Cal	Calculation
ch	Choke
cl	Clearance
cr	Critical
d	Design condition
dif	Entrance diffusion
df	Disc friction
Euler	Theoretical parameter
Exp	Experiment
h	Hub parameter
i	Impeller
IGV	Inlet guide vane
inc	Incidence
int	Internal condition
lk	Leakage
m	Meridional direction
mix	Mixing
par	Parasitic condition
re	Recirculation
rvd	Radial vaned diffuser
s	Shock; stage
sf	Skin friction
t	Tip parameter
th	Throat parameter
u	Tangential component
vB	Blockage friction in vaned diffuser
vch	Choke in vaned diffuser
vin	Incidence in vaned diffuser
vld	Vaneless diffuser
vsf	Skin friction in vaned diffuser
vw	Wake mixing in vaned diffuser
_	Averaged parameter

Superscripts

*	Sonic flow condition

pressors. Thanapandi and Prasad [9] surveyed a number of available loss correlations and found a satisfactory set of loss correlations for almost the full range of operating conditions of low specific speed submersible pumps. The loss correlation set also contains the shock loss. Aungier [10] presented a performance prediction method which doesn't account for shock loss, but the pressure ratio of the centrifugal compressor stage is only 3.5 and targets performance prediction under the design condition. Gong and Chen [11] combined all potential losses in each component of the device to reveal the full total pressure loss mechanism in a centrifugal compressor with volute. They proposed a set of loss correlations by reviewing the existing 1D loss correlations, which includes the Aungier's shock loss correlation, but the pressure ratio of the compressor stage only reaches 2.2. At present, high-pressure-ratio and highly-loaded centrifugal compressors are commonly applied, but their loss correlation sets don't predict their performance with sufficient accuracy. There is yet demand for a more accurate and reliable loss correlation set.

This paper proposes a new loss correlation selection method which works according to the inlet tip relative Mach number (M_{w2t}) and specific speed (n_s). The proposed method is validated with experimental results on eight centrifugal compressors in public and one in-house and compared with Oh's set.

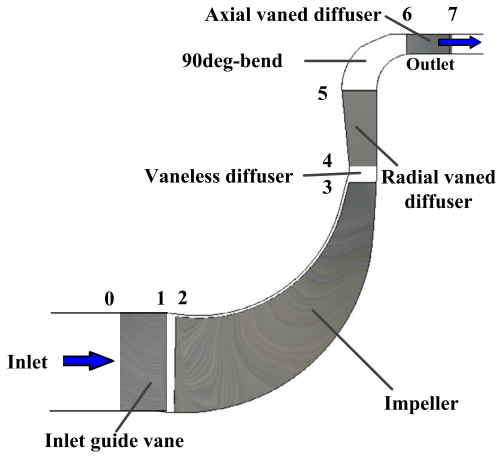

Fig. 1. Schematic of centrifugal compressor.

2. Reviews of loss mechanisms and correlation for centrifugal compressor

In this study, the compressor is divided into six individual components for modeling purposes as shown in Fig. 1 and Fig. 2. Each component inlet and exit is defined as a station. The compressor has eight stations (marked from 0 to 7). Station 0 and Station 1 fall at the inlet and outlet of the inlet guide vane (IGV). Due to the rotational domain, the impeller inlet is defined as Station 2. Station 3 is at the impeller outlet. The conditions for the impeller outlet and vaneless diffuser (VLD) inlet are the same. Station 4 is at the VLD outlet or the radial vaned diffuser (RVD) inlet. The RVD outlet and 90deg-bend inlet have the same conditions. Station 5 is at the RVD outlet or the 90deg-bend inlet. The 90deg-bend outlet and axial vaned diffuser (AVD) inlet have the same conditions. Station 6 is at the 90deg-bend outlet or the AVD inlet, and Station 7 is at the AVD outlet. In this model, if the compressor geometry and boundary conditions (total pressure and total temperature at the inlet, mass flow at the outlet, and rotational speed) are given, compressor performance indicators such as total pressure ratio and total-to-total isentropic efficiency are obtainable.

As discussed above, impeller losses described in the literature are internal or parasitic. Internal losses include skin friction loss, blade loading loss, mixing loss, tip clearance loss, incidence loss, entrance diffusion loss, choke loss and shock loss. Parasitic losses consist of disk friction loss, leakage loss and recirculation loss. In addition to losses in the impeller, enthalpy loss occurs in the inlet guide vane, vaneless diffuser and vaned diffuser. Each loss mechanism has one or more corresponding loss correlations as shown in Table 1. These loss correlations were taken from the literature under the following criteria: 1) the loss correlation frequently quoted is suitable for 1D calculation; 2) any loss correlation proved inaccurate has been excluded; 3) the loss correlation is excluded if it contains empirical coefficients that are widely and uncertainly valued.

Table 1
List of the corresponding loss correlations.

Loss mechanism	Loss correlation	Amount
Inlet guide vane diffuser	Galvas [1,12]	1
Skin friction loss	Jansen [13]	1
Blade loading loss	Coppage [14], Aungier [10]	2
Mixing loss	Johnston and Dean [15], Aungier [10]	2
Tip clearance loss	Rodgers [16], Krylov and Spunde [17], Jansen [13]	3
Incidence loss	Conrad [2], Aungier [10], Galvas [1]	3
Entrance diffusion loss	Aungier [10]	1
Choke loss	Aungier [10]	1
Shock loss	Aungier [10], Whitfield and Baines [3]	2
Disk friction loss	Daiy and Nece [18], Shepherd [19], Boyce [20]	3
Recirculation loss	Coppage [14], Oh [4]	2
Leakage loss	Aungier [10], Jansen [13]	2
Vaneless diffuser loss	Stanitz [21]	1
Radial vaned diffuser loss	Aungier [10]	1
90deg-bend loss	Aungier [10]	1
Axial vaned diffuser loss	Galvas [1,12]	1

2.1. Inlet guide vane loss

Loss in the axial turbine stator is associated with the fluid kinetic energy, boundary layer thickness and blade geometrical structure of the device [22]. According to Galvas [1,12], the loss mechanism of the inlet guide vane is similar to that of the axial turbine stator. The loss correlation for the axial turbine stator loss can be used to calculate the inlet guide vane loss. The inlet guide vane loss is computed as a fraction of the ideal kinetic energy as shown in Eq. (1). The kinetic energy fraction is associated with the exit flow angle of the inlet guide vane:

$$\Delta h_{IGV} = e_{s,IGV}(KE)_{id,1} \tag{1}$$

kinetic energy fraction

$$e_{s,IGV} = \frac{0.0076}{\cos\alpha_1 - 0.025}\left[1 + \frac{\cos(\alpha_1/2)}{0.7}\right] \tag{2}$$

ideal kinetic energy

$$(KE)_{id,1} = \frac{V_1^2}{2(1 - e_{s,IGV})} \tag{3}$$

2.2. Impeller loss

2.2.1. Skin friction loss

Skin friction loss is caused by the shear force on the channel surface. The loss correlation as Eq. (4) [13] is based on the assumption of pipe flow. This loss correlation excludes the effect of the non-uniform velocity distribution in the impeller channel due to the boundary layer:

$$\Delta H_{sf} = 2C_{f,i}\frac{L_b}{D_{hyd}}\overline{W}^2 \tag{4}$$

skin friction coefficient

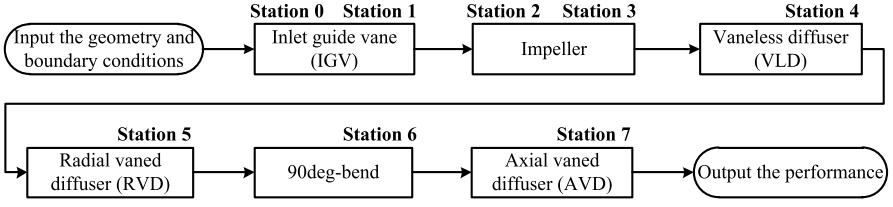

Fig. 2. Compressor components division.

$$C_{f,i} = 0.0412\,\mathrm{Re}^{-0.1925} \tag{5}$$

$$\mathrm{Re} = \frac{U_3 D_{hyd}}{\upsilon_{02}} \tag{6}$$

average relative velocity

$$\overline{W} = \frac{W_{2t} + W_{2h} + 2W_3}{4} \tag{7}$$

impeller flow length

$$L_b = \frac{\pi}{8}\left(d_3 - \frac{d_{2t}+d_{2h}}{2} - b_3 + 2L_z\right) \times \left(\frac{2}{\frac{\cos\beta_{2t}+\cos\beta_{2h}}{2} + \cos\beta_3}\right) \tag{8}$$

impeller average hydraulic diameter

$$D_{hyd} = \frac{d_3\cos\beta_3}{(\frac{Z}{\pi} + \frac{d_3\cos\beta_3}{b_3})} + \frac{\frac{1}{2}(\frac{d_{2t}}{d_3} + \frac{d_{2h}}{d_3})(\frac{\cos\beta_{2t}+\cos\beta_{2h}}{2})}{\frac{Z}{\pi} + (\frac{d_{2t}+d_{2h}}{d_{2t}-d_{2h}})(\frac{\cos\beta_{2t}+\cos\beta_{2h}}{2})} \tag{9}$$

2.2.2. Blade loading loss

In the flow passage, there is a negative velocity gradient near the blade surface, which leads to boundary layer growth and flow separation. This phenomenon results in blade loading loss. Coppage [14] thought that flow diffusion is the main cause of boundary layer growth. He proposed the following equation to calculate the blade loading loss:

$$\Delta H_{bl} = 0.05 D_f^2 U_3^2 \tag{10}$$

diffusion factor

$$D_f = 1 - \frac{W_3}{W_{2t}} + \frac{0.75\Delta H_{Euler} W_3}{[\frac{Z_3}{\pi}(1 - \frac{d_{2t}}{d_3}) + \frac{2d_{2t}}{d_3}]W_{2t}U_3^2} \tag{11}$$

theoretical head enthalpy

$$\Delta H_{Euler} = U_3 C_{3u} - U_2 C_{2u} \tag{12}$$

Aungier [10] asserted that the blade-to-blade pressure gradient produces a strong secondary flow and blade loading loss. He presented the loss correlation as Eq. (13) to calculate the blade loading loss, as a function of the relative velocity difference between the suction and pressure side:

$$\Delta H_{bl} = \frac{\Delta W^2}{48} \tag{13}$$

$$\Delta W = \frac{2\pi d_3 V_{3u}}{Z L_b} \tag{14}$$

2.2.3. Mixing loss

As the flow fully diffuses, high aerodynamic blockage is inevitable at the impeller outlet. This leads to a low momentum fluid and a high energy region at the impeller outlet called a "jet and wake" flow pattern. Ali [23] found the wake exists in the corner where the suction side and the shroud meet. Mixing loss occurs due to the mixing of the jet and wake flow at the impeller outlet.

Johnston and Dean [15] asserted that jet flow mixing with wake flow at the impeller outlet is a rapid expansion process, i.e., the wake disappears at the radius very close to the impeller exit radius. They treated the exit velocity distribution with a square-wave profile, and assumed no change in the relative velocity along the passage depth direction. They also assumed that static pressure in the jet and wake are the same at the impeller outlet and there is no relative flow in the wake. As the mixing loss correlation suggested by Johnston and Dean (Eq. (15)), wake width markedly affects mixing loss. This is applicable in highly-loaded centrifugal compressors with clear-cut "jet and wake" structure:

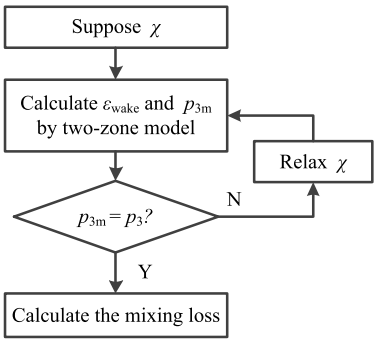

Fig. 3. Width of wake flow solving process.

$$\Delta H_{mix} = \frac{1}{1+\tan^2\alpha_3}\left(\frac{1-\varepsilon_{wake}-b^*}{1-\varepsilon_{wake}}\right)^2 \frac{V_3^2}{2} \tag{15}$$

Where ε_{wake} represents wake width, ranging from 0.366 to 0.482 [24]. According to our previous study [25], wake width is determined by two-zone model and conducted by an iterative solution to converge on the static pressure at the impeller outlet as showed in Fig. 3.

Step1 Suppose the wake mass fraction χ, ranging from 0.15 to 0.25.

Step2 Calculate the wake width ε_{wake} and static pressure p_{3m} by two-zone model.

Step3 Calculate the relative error between the static pressurep_{3m} and the static pressure p_3 calculated by 1D calculation. If the error is less than 10^{-5}, turn to **Step4**. Otherwise, relax the wake flow mass fraction χ and turn to **Step2**.

Step4 Calculate the mixing loss used to compute impeller loss.

Once flow separation occurs, there is no further diffusion in the impeller channel. Aungier [10] stated accordingly that the wake flow mixes with jet flow at velocity W_{sep}. If the equivalent diffusion factor $D_{eq} > 2$, separation is assumed to occur inside the flow passage. The relative velocity difference between the separation point and the impeller outlet can be used to evaluate the mixing loss. Aungier [10] suggested that the mixing loss correlation could be written as equation below.

$$\Delta H_{mix} = 0.5(W_{sep} - W_{out})^2 \tag{16}$$

where

$$W_{sep} = \begin{cases} W_3 & D_{eq} \le 2 \\ W_3 D_{eq}/2 & D_{eq} > 2 \end{cases} \tag{17}$$

$$W_{out} = \sqrt{\left[V_{3m}A_3/(\pi d_3 b_3)\right]^2 + W_{2u}^2} \tag{18}$$

$$D_{eq} = \frac{W_{\max}}{W_3} \tag{19}$$

$$W_{\max} = \frac{W_2 + W_3 + \Delta W}{2} \tag{20}$$

2.2.4. Tip clearance loss

For unshrouded impeller, there is a small clearance between the blade tip and casing that allows the impeller to rotate freely. Tip clearance loss results from the leakage flow through the tip clearance mixing with the main flow, where there is a pressure difference between the suction and pressure side [26]. Rodgers [16] thought the tip clearance loss is mainly dependent on the tip clearance size. The estimation of this loss is computed using the following loss correlation, as a function of the ratio of the tip clearance size to the impeller exit width:

$$\Delta H_{cl} = 0.1\frac{c}{b_3}U_3^2 \tag{21}$$

Krylov and Spunde [17] also presented a loss correlation as Eq. (22) to evaluate clearance loss. Unlike the Rodgers correlation, this loss correlation takes the ratio of inlet to outlet radius into account.

$$\Delta H_{cl} = 2\frac{c}{b_3}\left(\frac{r_{2h}+r_{2t}}{2r_3} - 0.275\right)U_3^2 \tag{22}$$

Jansen [13] found that the fluid experiences a rapid contraction and expansion process through the tip clearance. He established a loss correlation (Eq. (23)) to calculate the clearance loss by considering the ratio of inlet to outlet density, unlike the two correlations mentioned above:

$$\Delta H_{cl} = 0.6\frac{c}{b_3}V_{3u}\left(\frac{4\pi}{b_3 Z}\frac{r_{2t}^2 - r_{2h}^2}{r_3 - r_{2t}}V_{3u}V_2/\left(1+\frac{\rho_3}{\rho_2}\right)\right)^{1/2} \tag{23}$$

2.2.5. Incidence loss

Incidence loss occurs when the inlet relative flow angle β_2 differs from the inlet blade angle β_{2b}. In this case, the flow must change the direction rapidly in keeping with the inlet blade angle, which readily causes flow separation. Conrad [2] found the incidence loss is proportional to the tangential relative velocity squared at the impeller outlet. The loss correlation can be written as follows:

$$\Delta H_{inc} = f_{inc}W_{2u}^2/2 \tag{24}$$

where f_{inc} represents the incidence coefficient, ranging from 0.5 to 0.7. In this study, f_{inc} is averaged, and valued as 0.6.

Aungier [10] also proposed an incidence loss correlation where the flow direction is axial at the impeller inlet. The loss is evaluated by the difference between actual and ideal relative velocity:

$$\Delta H_{inc} = 0.4(W_2 - V_{2m}/\cos\beta_{2b})^2 \tag{25}$$

Galvas [1] thought the incidence loss is related to the difference between the actual flow angle and the optimum flow angle at the impeller inlet. He proposed a loss correlation as Eq. (26):

$$\Delta H_{inc} = \frac{W_L^2}{2C_p} \tag{26}$$

$$W_L = W_{2m}\cos|\beta_{opt} - \beta_2| \tag{27}$$

The optimum flow angle is calculated from the inlet velocity diagram characteristics and blade blockage at the RMS diameter [27]:

$$\beta_{opt} = \beta_{2b} - \varepsilon_2 \tag{28}$$

$$\tan\varepsilon_2 = \frac{(1-B_2)\tan\beta_2}{1+B_2\tan^2\beta_2} \tag{29}$$

$$B_2 = 1 - \frac{Z_2 t_2}{\pi d_2 \sin\beta_{2b}} \tag{30}$$

2.2.6. Entrance diffusion loss

For certain impellers, incidence loss correlations occasionally underestimate the entrance loss at the positive incidence angles. The flow adjustment between the leading edge and throat has more significant effect on the entrance loss. Entrance diffusion loss can be calculated by Eq. (31) according to Aungier [10]:

$$\Delta H_{dif} = 0.4(W_2 - W_{th})^2 - \Delta H_{inc} \tag{31}$$

If the entrance diffusion loss calculated is negative, it is valued as zero.

Kosuge [28] found that entrance diffusion loss should be limited by a value, when inducer stall occurs. With a variety of public test data, Aungier [10] found that inducer stall occurs when the flow diffusion from inlet to throat exceeds 1.75:

$$\Delta H_{dif} \geq 0.5(W_{2t} - 1.75W_{th})^2 - \Delta H_{inc} \tag{32}$$

$$W_{2t}/W_{th} > 1.75 \tag{33}$$

2.2.7. Choke loss

Mass flow is maximized when fluid flows through the impeller throat at the speed of sound. If the mass flow continues to increase, the centrifugal compressor performance will drop rapidly due to choke loss. Aungier [10] related the choke loss with the geometrical structure and aerodynamic blockage in the impeller throat to form the following correlation:

$$\Delta H_{ch} = \begin{cases} \frac{1}{2}W_2^2(0.05X + X^7) & X > 0 \\ 0 & X \leq 0 \end{cases} \tag{34}$$

$$X = 11 - 10(C_r A_{th})/A_{th}^* \tag{35}$$

where A_{th}^* represents the impeller's throat area for which the assigned mass flow will yield a sonic velocity.

Aerodynamic blockage is evaluated by the contraction ratio calculated as follows

$$C_r = \sqrt{A_2\cos\beta_{2b}/A_{th}} \tag{36}$$

where the C_r is limited that $C_r \leq 1 - (A_2\cos\beta_{2b}/A_{th} - 1)^2$.

2.2.8. Shock loss

There is a shock wave in the inlet suction side of the transonic impeller. The total pressure loss is related to fluid flowing across the shock wave [29]. Aungier [10] calculated the shock loss as Eq. (37) according to the difference between the actual and critical inlet relative Mach number:

$$\Delta H_s = 0.2\left[(M_{w2} - M_{w2cr})W_{\max}\right]^2 \tag{37}$$

Inlet critical relative Mach number

$$M_{w2cr} = M_{w2}W^*/W_{\max} \tag{38}$$

where W^* represents the local sonic velocity.

Whitfield and Baines [3] thought that shock loss is caused by a normal shock wave at the impeller inlet which produces the following loss correlation. Shock loss in this case mainly depends on the ratio of the throat to the inlet relative velocity and the ratio of the throat to the inlet static pressure:

$$\Delta H_s = \frac{W_2^2}{2}\left\{1 - \left(\frac{W_{th}}{W_2}\right)^2 - \left(\frac{2}{(\gamma-1)M_{w2}^2}\right) \times \left[\left(\frac{p_{th}}{p_2}\right)^{\frac{\gamma}{\gamma-1}} - 1\right]\right\} \tag{39}$$

2.2.9. Disk friction loss

Disk friction loss results from the shear forces between the disk and housing. The geometrical structure of the impeller and housing significantly affects the loss. Daily and Nece [18] conducted an experimental study, where a smooth plane disk rotated within a right-cylindrical chamber. They analyzed the experimental phenomena to establish the following loss correlation to predict the disk friction loss:

$$\Delta H_{df} = f_{df}(\rho_2 + \rho_3) r_3^2 U_3^3 / (8m) \tag{40}$$

Disk friction factor

$$f_{df} = \begin{cases} 2.67/(\mathrm{Re}_{df})^{0.5} & \mathrm{Re}_{df} < 3 \times 10^5 \\ 0.0622/(\mathrm{Re}_{df})^{0.2} & \mathrm{Re}_{df} \geq 3 \times 10^5 \end{cases} \tag{41}$$

$$\mathrm{Re}_{df} = U_3 r_3 / \nu_3 \tag{42}$$

Shepherd [19] also proposed a model as below

$$\Delta H_{df} = 0.01356 \rho_3 U_3^3 D_3^2 / \left(m\,\mathrm{Re}^{0.2}\right) \tag{43}$$

where $\mathrm{Re} = U_3 d_3 / \nu_{02}$.

Boyce [20] suggested the model expressed as follows to calculate the disk friction loss:

$$\Delta H_{df} = f_{df}\left(1 + \frac{p_3}{p_2}\right) \frac{\Delta H_{Euler}}{2} \frac{V_2}{U_3} \frac{r_3^2}{r_{2t}} \left(1 - \left(\frac{r_{2h}}{r_3}\right)^2\right) \tag{44}$$

2.2.10. Recirculation loss

Recirculation loss is caused by flow backing into the impeller and is affected by the diffusion factor and exit absolute flow angle. In a high-pressure and highly-loaded centrifugal compressor, high recirculation loss occurs due to the large exit absolute flow angle and high diffusion factor. The correlation below was established by Coppage [14]:

$$\Delta H_{re} = 0.02 \sqrt{\tan \alpha_3} D_f^2 U_3^2 \tag{45}$$

Oh [4] examined the exit absolute flow angle and built the recirculation loss correlation shown in Eq. (46), where a hyperbolic functional form was applied. The loss correlation was validated with experimental results using low pressure ratio centrifugal compressors, but it doesn't function properly for highly-loaded centrifugal compressors:

$$\Delta H_{re} = 8 \times 10^{-5} \sinh\left(3.5\alpha_3^3\right) D_f^2 U_3^2 \tag{46}$$

2.2.11. Leakage loss

Leakage loss results from the leakage flow through the centrifugal compressor seals to the low pressure regions. For unshrouded impellers, the loss occurs in the disk/housing gap. The loss can be calculated by correlations given by Aungier [10] and Jansen [13] as Eq. (47) and Eq. (48), respectively:

$$\Delta H_{lk} = \rho_3 c U_3 1.332 \left(r_3 V_{3u} - (r_2 V_{2u})_m\right) / (2\bar{r}\bar{b}) \tag{47}$$

$$\Delta H_{lk} = 0.6 \frac{c}{b_3} V_3 \sqrt{\frac{4\pi}{b_3 Z} \frac{\frac{r_{2t} - r_{2h}}{r_3 - r_{2t}}}{1 + \frac{\rho_3}{\rho_2}} V_{3u} V_2} \tag{48}$$

2.3. Diffuser system loss

2.3.1. Vaneless diffuser loss

There is always a vaneless space directly following the impeller within which the flow continually diffuses regardless of whether the compressor has a diffuser. The flow results in enthalpy loss in the vaneless space due to friction and diffusion. According to the mass, momentum and energy conservation developed by Stanitz [21], the flow solution is achieved by Runge-Kutta integration. The skin friction loss coefficient $C_{f,vld}$ related to Re can be expressed as follows [30]:

$$C_{f,vld} = k\left(1.8 \times 10^5 / \mathrm{Re}\right)^{0.2} \tag{49}$$

$$\mathrm{Re} = \frac{VD}{\nu} \tag{50}$$

Stanitz [21] developed a correlation to evaluate the enthalpy loss in the vaneless diffuser:

$$\Delta H_{vld} = C_p T_{03} \left[\left(\frac{p_4}{p_{04}}\right)^{\frac{\gamma-1}{\gamma}} - \left(\frac{p_4}{p_{03}}\right)^{\frac{\gamma-1}{\gamma}} \right] \tag{51}$$

2.3.2. Radial vaned diffuser loss

Aungier [31] found that radial vaned diffuser loss consists of dominant incidence loss and other four types of losses as shown in Eq. (52).

$$\Delta H_{rvd} = \Delta H_{vin} + \Delta H_{vsf} + \Delta H_{vch} + \Delta H_{vB} + \Delta H_{vw} \tag{52}$$

Incidence loss

$$\Delta H_{vin} = \begin{cases} 0.4(V_4 - V_4^*)^2 & V_4 < V_{4s} \\ 0.4[V_4^2 - V_{4s}^2 + (V_{4s} - V_4^*)^2] & V_4 \geq V_{4s} \end{cases} \tag{53}$$

where V_4^* represents the inlet velocity of the radial vaned diffuser at the optimum incidence. V_{4s} represents the inlet velocity at the stall incidence.

The optimum incidence angle is defined as

$$\cos \alpha_4^* = V_{4m} / V_4^* = \sqrt{\cos \alpha_{4b} \cos \alpha_{th,rvd}} \tag{54}$$

$$\cos \alpha_{th,rvd} = A_{th,rvd} / A_4 \tag{55}$$

Skin friction loss

$$\Delta H_{vsf} = C_{f,rvd} \frac{L_{vb}}{D_{vhyd}} \overline{V_{rvd}}^2 \tag{56}$$

where D_{vhyd} represents the average hydraulic diameter of the radial vaned diffuser and is an average of the throat and discharge values. It is computed similarly to the impeller, using Eq. (9).

Choke loss

$$\Delta H_{vch} = \begin{cases} 0 & X_{rvd} \leq 0 \\ \frac{1}{2} V_4^2 (0.05 X_{rvd} + X_{rvd}^7) & X_{rvd} > 0 \end{cases} \tag{57}$$

$$X_{rvd} = 11 - 10(C_{r,rvd} A_{th,rvd}) / A_{th,rvd}^* \tag{58}$$

$$C_{r,rvd} = \sqrt{A_4 \cos \alpha_{4b} / A_{th,rvd}} \tag{59}$$

where $A_{th,rvd}^*$ represents the throat area of radial vaned diffuser for which the assigned mass flow will yield a sonic velocity.

Discharge blockage friction loss

$$\Delta H_{vB} = \frac{1}{2} \left(\frac{V_5}{1 - B_5} - V_5 \right)^2 \tag{60}$$

The discharge area blockage is defined as

$$B_5 = \left[K_1 + K_2 \left(\bar{C}_R^2 - 1\right)\right] L_{vb} / s_5 \tag{61}$$

$$\bar{C}_R = \frac{1}{2} \left(\frac{V_{m4} \cos \alpha_{5b}}{V_{m5} \cos \alpha_{4b}} + 1 \right) \tag{62}$$

$$K_1 = 0.2\left[1 - 1/(C_L / C_\theta)\right] \tag{63}$$

$$K_2 = \frac{2\theta_c}{125 C_\theta} \left[1 - \frac{2\theta_c}{22 C_\theta} \right] \tag{64}$$

Diffuser divergence angle

$$2\theta_c = 2\cot^{-1}\left\{\left[(s_5 - t_5)b_5/b_4 - s_4 + t_4\right]/(2L_{vb})\right\} \tag{65}$$

Blade to blade width

$$s = (\pi d \cos\alpha_b)/Z_{rvd} \tag{66}$$

Wake mixing loss

$$\Delta H_{vw} = \frac{1}{2}(V_{sep,rvd} - V_{out,rvd})^2 \tag{67}$$

$$V_{sep,rvd} = V_5/(1 + 2C_{\theta,rvd}) \tag{68}$$

$$V_{out,rvd} = \sqrt{\left[V_{5m}A_5/(\pi d_5 b_5)\right]^2 + V_{5u}^2} \tag{69}$$

where $C_{\theta,rvd}$ and $C_{L,rvd}$ represents the empirical blockage correction factor.

2.3.3. 90deg-bend loss

Unlike vaneless diffuser loss, 90deg-bend loss encompasses the loss due to passage curvature. Stanitz's vaneless diffuser model takes no curvature effect into consideration. In this study, Aungier's [32] vaneless space model is used to account for the curvature effect. The loss correlation as below can be used to evaluate the enthalpy loss in the 90deg-bend.

$$\Delta H_b = C_p T_{03}\left[\left(\frac{p_6}{p_{06}}\right)^{\frac{\gamma-1}{\gamma}} - \left(\frac{p_6}{p_{05}}\right)^{\frac{\gamma-1}{\gamma}}\right] \tag{70}$$

2.3.4. Axial vaned diffuser loss

Aungier's vaned diffuser model is also suitable for airfoil style vaned diffusers [33]. Therefore, the radial diffuser model in the paper is also applicable to the axial vaned diffuser.

2.4. Slip factor model

Due to the limited blade number and friction effect, the exit relative flow angle β_3 differs from the exit blade angle β_{3b}. For centrifugal impellers, this deviation can be evaluated using a slip factor. Many slip factor models have been proposed by Stodola [34], Stanitz [21], Wiesner [35], Qiu [36], etc. Qiu's model is unsuitable due to the unknown blade turning term in 1D preliminary design. According to our previous study [37] and the study of Wiesner [35], compared with Stodola's and Stanitz's model, more accurate Wiesner's model is adopted expressed as follows

$$\mu = 1 - \sqrt{\cos\beta_{3b}}/Z_3^{0.7} \tag{71}$$

2.5. Blockage factor model

In general, aerodynamic blockage at the impeller inlet is assumed to be thin as zero. Since the flow has diffused fully, high aerodynamic blockage always occurs at the impeller outlet. Aerodynamic blockage at the impeller outlet varies with the area ratio and diffusion ratio. The effect of tip clearance is additionally included in the model of JongSik Oh [38].

$$B_3 = 0.02AR + 0.03DR^3 + \frac{c_3}{b_3} \tag{72}$$

$$AR = \frac{2\pi r_3 b_3 - Z_3 b_3 t_3/\cos\beta_{3b}}{b_2(2\pi r_2 \cos\beta_{2b} - Z_2 t_2)} \tag{73}$$

$$DR = \frac{\overline{W_2}}{\overline{W_3}} \tag{74}$$

2.6. Overall performance calculation

For each component as shown in Fig. 2, the inlet, throat and outlet flow conditions can be determined by the static density iteration. The flow from inlet to throat is assumed to be an isentropic process for subsonic impellers and treated as a polytropic process for transonic impellers when shock loss is considered [39]. The flow from inlet to outlet is a polytropic process considering the component losses. The flow conditions at the outlet can be determined through static density iteration with loss correlations. Once the iterative solution is to be converged within a specified tolerance for all components, the centrifugal compressor performance can be assessed as follows:

Stage total-to-total isentropic efficiency

$$\eta_s = \frac{\Delta H_{Euler} - \Delta H_{int} - \Delta H_{IGV} - \Delta H_D}{\Delta H_{Euler} + \Delta H_{par}} \times 100\% \tag{75}$$

Impeller total-to-total isentropic efficiency

$$\eta_i = \frac{\Delta H_{Euler} - \Delta H_{int}}{\Delta H_{Euler} + \Delta H_{par}} \times 100\% \tag{76}$$

Inlet guide vane loss percentage for stage

$$Loss_{IGV} = \frac{\Delta H_{IGV}}{\Delta H_{Euler} + \Delta H_{par}} \times 100\% \tag{77}$$

Impeller internal loss percentage for stage

$$Loss_{i,int} = \frac{\Delta H_{int}}{\Delta H_{Euler} + \Delta H_{par}} \times 100\% \tag{78}$$

Impeller parasitic loss percentage for stage

$$Loss_{i,par} = \frac{\Delta H_{par}}{\Delta H_{Euler} + \Delta H_{par}} \times 100\% \tag{79}$$

Diffuser system loss percentage for stage

$$Loss_D = \frac{\Delta H_D}{\Delta H_{Euler} + \Delta H_{par}} \times 100\% \tag{80}$$

The impeller internal head enthalpy is defined as

$$\Delta H_{int} = \Delta H_{sf} + \Delta H_{bl} + \Delta H_{mix} + \Delta H_{cl} + \Delta H_{inc} + \Delta H_{dif} + \Delta H_{ch} + \Delta H_s \tag{81}$$

The parasitic head enthalpy is defined as

$$\Delta H_{par} = \Delta H_{df} + \Delta H_{re} + \Delta H_{lk} \tag{82}$$

The diffuser system head enthalpy loss is defined as

$$\Delta H_D = \Delta H_{vld} + \Delta H_{rvd} + \Delta H_b + \Delta H_{avd} \tag{83}$$

Stage total pressure ratio is calculated by equation as below:

$$PR_s = \left(1 + \eta_s\left(\frac{T_{03} - T_{02}}{T_{02}}\right)\right)^{\frac{\gamma}{\gamma-1}} \tag{84}$$

Impeller total pressure ratio is calculated by equation as below:

$$PR_i = \left(1 + \eta_i\left(\frac{T_{03} - T_{02}}{T_{02}}\right)\right)^{\frac{\gamma}{\gamma-1}} \tag{85}$$

Table 2
Design parameters of eight centrifugal compressors.

Impeller	Impeller (A) [40–42]	Impeller (B) [43,44]	Impeller (C) [45]	Impeller (D) [4]	Impeller (E) [46]	Impeller (F) [46]	Impeller (G) [47]	Impeller (H) [48,49]
Inlet hub diameter d_{2h}/mm	90	60	63.96	45	90	90	20	44.6
Inlet tip diameter d_{2t}/mm	225.5	156	112.5	95.3	280	280	61	97.2
Inlet hub blade angle β_{2h}/deg	31.4	37.0	53.9	34.2	32	32	31	46.6
Inlet tip blade angle β_{2t}/deg	63.3	63.5	62.2	56.3	63	63	46	61.5
Exit diameter d_3/mm	400	224	208	207.4	400	400	90	163.4
Exit blade width b_3/mm	14.71	10.2	7.57	7.5	26	26	6.5	4.90
Exit blade angle β_{3b}/deg	30	38	30.2	30	0	30	30	34
Impeller axial length L_z/mm	119.84	75.15	37.02	75	130	130	32	47.32
Exit blade number Z_3	24	13 + 13	18 + 18	12	20	20	7 + 7	19
Mass flow m (kg/s)	4	2.55	0.90	0.3	5.32	4.54	0.35	0.98
Rotational speed/rpm	22363	50000	45337	15000	14000	14000	80000	68384
Pressure ratio	4.07	6.1	5.5	1.18	2.1	1.91	2.24	7.1
Isentropic efficiency/%	84.56	84.25	91.30	–	88.15	88.14	79.00	89.50
Tip clearance size/mm	0.2	0.3	0.174	0.2	0.525	0.525	0.27	0.191
Exit vaneless diffuser diameter d_4/mm	560	358.4	232	370	680	680	148	–
Inlet tip relative Mach no. M_{w2t}	0.92	1.3	0.87	0.26	0.65	0.64	0.83	1.25
Specific speed n_s	0.531	0.812	0.463	0.603	0.723	0.748	0.988	0.636
Specific diameter d_s	4.397	3.266	5.011	4.561	3.104	3.236	2.787	3.945

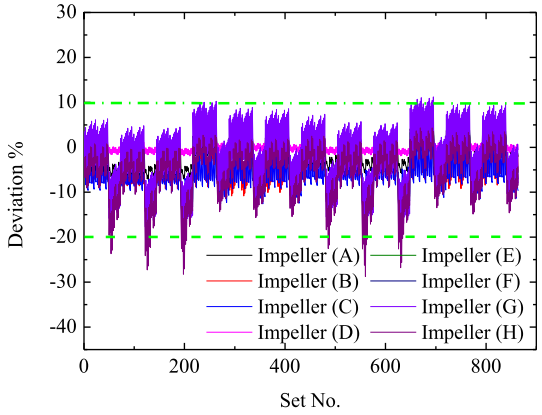

Fig. 4. Isentropic efficiency deviation for 864 loss correlation sets.

3. Loss correlation selection

In the present study, each loss mechanism has one or more corresponding loss correlations as shown in Table 1. There are 864 loss correlation sets which are obtained by permutation and combination. These loss correlation sets predict the performance of eight centrifugal compressors with the geometrical and performance parameters detailed in Table 2. The experimental impeller performance data of Impeller (H) is available. For Impellers (A)–(G), stage experimental performance data is available but there is no stage experimental performance data under the design condition for Impellers (B) or (C).

As shown in Fig. 4, the maximum deviation between the predicted isentropic efficiency and experimental value under the design condition is up to 20%. It is necessary to find a reliable loss correlation set to predict centrifugal compressor performance with sufficient accuracy.

For high-pressure-ratio and highly-loaded centrifugal compressors, the interaction of the shock wave with the boundary layer and tip leakage flow markedly impacts the flow in the impeller [50,51]. The shock wave not only can produce shock loss, but also affect other losses. The loss correlation set of transonic centrifugal compressors should differ from that of subsonic centrifugal compressors accordingly. The inlet tip relative Mach number (M_{w2t}) defined by Eq. (89) is used to confirm whether or not there is a shock wave. Inlet tip relative Mach number higher than 0.8 is used as a criterion for transonic centrifugal compressors.

$$M_{w2t} = \frac{W_{2t}}{\sqrt{\gamma R_g T_2}} \tag{86}$$

The centrifugal compressor loss is mainly affected by the geometric structure and enthalpy change. The specific speed (n_s) represents the non-dimensional rotational speed (Eq. (90)), a function of the rotational speed, volume flow rate and isentropic head rise [52]. The specific speed relates to the geometrical parameters, e.g., inlet to outlet radius ratio. When the specific speed is high, the specific diameter is low according to the Cordier line [52]. The interaction of the shock wave with the boundary layer has more impact on the flow condition of the low specific diameter impeller, compared to that of the high specific diameter impeller. The specific speed is used here to select the loss correlation for transonic centrifugal impellers. The critical specific speed value (0.7) is determined by testing multiple loss correlations:

$$n_s = \frac{2\pi n}{60} \frac{(Q_2)^{0.5}}{(\Delta h_{0s})^{0.75}} \tag{87}$$

Isentropic total enthalpy rise

$$\Delta h_{0s} = C_p T_{02}\left[(PR)^{\frac{\gamma}{\gamma-1}} - 1\right] \tag{88}$$

Volume flow rate

$$Q_2 = \frac{m}{\rho_{02}} \tag{89}$$

The prediction results of 864 loss correlation sets combined with the inlet tip relative Mach number (M_{w2t}) and specific speed (n_s) were used to develop a new method to select loss correlations. When $M_{w2t} < 0.8$, Set 1 is selected; when $M_{w2t} \geq 0.8$ & $n_s < 0.7$, Set 2 is selected; when $M_{w2t} \geq 0.8$ & $n_s \geq 0.7$, Set 3 is selected. The three loss correlation sets are shown in Table 3. Compared with Oh's set, entrance diffusion loss, choke loss and shock loss are considered in proposed method. Set 1 and Oh's set mainly are used to predict the lowly-loaded centrifugal compressor performance, and their blade loading, mixing, incidence, recirculation and leakage loss correlations are different. For Sets 1–3, their blade loading, mixing, clearance and leakage loss correlations are different.

4. Results and discussions

The proposed loss correlation selection method was used to predict the performance of eight centrifugal compressors. The

Table 3
Loss correlation sets.

Loss mechanism	Set 1	Set 2	Set 3	Oh's Set [4]
Inlet guide vane diffuser	Galvas	Galvas	Galvas	Galvas
Skin friction loss	Jansen	Jansen	Jansen	Jansen
Blade loading loss	Aungier	Coppage	Aungier	Coppage
Mixing loss	Aungier	Johnston and Dean	Aungier	Johnston and Dean
Clearance loss	Jansen	Jansen	Rodgers	Jansen
Incidence loss	Aungier	Aungier	Aungier	Conrad
Entrance diffusion loss	Aungier	Aungier	Aungier	None
Choke loss	Aungier	Aungier	Aungier	None
Shock loss	None	Whitfield and Baines	Whitfield and Baines	None
Disk friction loss	Daiy and Nece	Daiy and Nece	Daiy and Nece	Daiy and Nece
Recirculation loss	Coppage	Coppage	Coppage	Oh
Leakage loss	Jansen	Aungier	Jansen	Aungier
Vaneless diffuser loss	Stanitz	Stanitz	Stanitz	Stanitz
Radial vaned diffuser loss	Aungier	Aungier	Aungier	Aungier
90deg-bend loss	Aungier	Aungier	Aungier	Aungier
Axial vaned diffuser loss	Aungier	Aungier	Aungier	Aungier

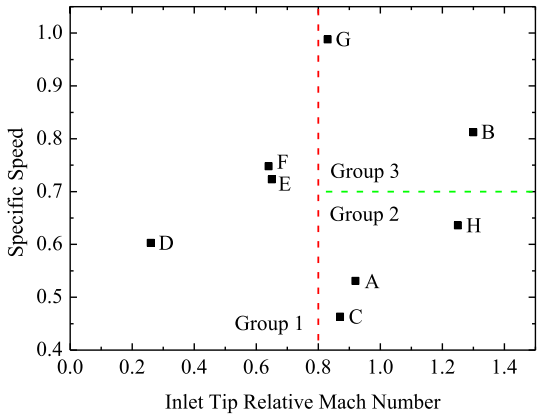

Fig. 5. The relationship between the specific speed and inlet tip relative Mach number.

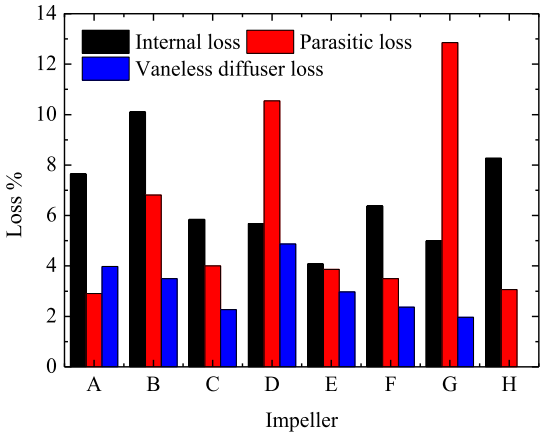

Fig. 6. Three types of losses comparison for eight centrifugal compressors.

stage performance of Impellers (A)-(G) and the impeller performance of Impeller (G) were predicted. According to the respective inlet tip relative Mach number (M_{w2t}) and specific speed (n_s) shown in Table 2, the eight centrifugal compressors were divided into three groups as shown in Fig. 5. Impellers (D), (E) and (F) in Group 1 are subsonic impellers as their inlet tip relative Mach number (M_{w2t}) are below 0.8. Others centrifugal impellers are transonic impellers. Group 2 contains Impellers (A), (C) and (H), due to their less specific speed (n_s) below 0.7. Group 3 contains Impellers (B) and (G) with high specific speed (n_s) over 0.7. Sets 1–3 were applied to predict the performance of Groups 1–3 in turn. The predicted results were compared with the experimental results to validate the proposed method under design and off-design conditions.

4.1. Design condition

There is no experimental data for stage performance under the design condition, so impeller performance comparisons were conducted for only Impellers (B), (C) and (H). There are no experimental results for stage isentropic efficiency, so only stage total pressure ratio prediction was conducted for Impeller (D). Table 4 shows the experimental isentropic efficiency versus the calculated isentropic efficiency under the design condition. Impellers marked means the impeller performance, and PR marked means the stage total pressure ratio. The efficiency predicted by the proposed method agrees well with the experimental efficiency with deviation below 1.20%. Oh's set predicts performance well in subsonic centrifugal compressors, but under-predicts greatly in transonic centrifugal compressors. It matches the conclusion mentioned above that Oh's set fails to predict the performance of highly-loaded centrifugal compressors. The main reason is too much high incidence loss and recirculation loss predicted by Oh' set. The details will be described next. Therefore, it is necessary to select different loss correlation sets for different types of centrifugal compressors and the proposed method to select loss correlation is reliable.

Fig. 6 shows the results of internal losses, parasitic losses and vaneless diffuser loss for eight centrifugal compressors under the design condition. The internal losses dominate the parasitic and vaneless diffuser loss for Impellers (A), (B), (C), (F) and (H) up to around 50%, 50%, 50%, 50% and 60% of total losses, in turn. If these centrifugal compressors need to be optimized, the geometrical parameters affecting the internal losses should be given priority. For Impellers (D) and (G), parasitic losses are the dominant losses affecting compressor performance and both exceed 50%. Recirculation loss is the major parasitic loss [4], so the high back flow at the impeller outlet needs to be cared for these impellers.

The loss distribution under the design condition for Impeller (A) is shown in Table 5. The underlined part represents the results of proposed method (Set 2) for Impeller (A) and the loss correlation for the same loss mechanism is labeled "No.". For example, for blade loading loss, No. 1 and 2 represent the loss correlations proposed by Coppage and Aungier, respectively. On the whole, the predicted results by different loss correlations for the same mechanism differ considerably, except for clearance loss. Due to the transonic impeller, Coppage's loss correlation is applied to predict the blade loading loss. It is significantly higher than that predicted

Table 4
Comparison between the experimental and predicted isentropic efficiency.

Impeller	Impeller (A)	Impeller (B)	Impeller (C)	Impeller (D) (PR)
Isentropic efficiency (Exp. %)	84.56	84.25 (impeller)	91.30 (impeller)	1.179
Isentropic efficiency (Present %)	85.47	83.08 (impeller)	90.15 (impeller)	1.182
Isentropic efficiency (Oh's Set %)	80.03	76.51 (impeller)	79.84 (impeller)	1.193
Deviation (Present %)	0.91	−1.17	−1.15	−0.25
Deviation (Oh's Set %)	−4.53	−7.74	−11.46	1.20
Impeller	Impeller (E)	Impeller (F)	Impeller (G)	Impeller (H)
Isentropic efficiency (Exp. %)	88.15	88.14	79.00	89.50 (impeller)
Isentropic efficiency (Present %)	89.08	87.76	80.18	88.66 (impeller)
Isentropic efficiency (Oh's Set %)	88.04	87.54	73.23	80.06 (impeller)
Deviation (Present %)	0.93	−0.38	1.18	−0.84
Deviation (Oh's Set %)	−0.11	−0.60	−5.77	−9.44

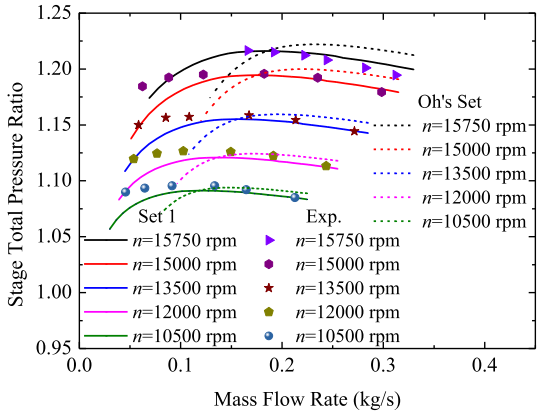

Fig. 7. Stage total pressure ratio prediction for Impeller (D).

by Aungier's loss correlation. For incidence loss, Cornard's loss correlation predicts a very high and unreasonable loss (up to 6.85%). Oh's loss correlation over-predicts recirculation loss (up to 2.92%), so they are inapplicable. Oh's set applies Cornard's incidence loss correlation and Oh's recirculation loss correlation, so the set fails to predict the performance of highly-loaded centrifugal compressors. According to the result of Set 2, recirculation loss dominates the parasitic losses. These results align with the literature [4], which indicates that the loss correlation set for Impeller (A) is reliable and that the proposed loss correlation selection method is suitable.

4.2. Off-design condition

There is no experimental data for stage performance under the off-design condition, so only impeller performance comparisons were conducted for Impeller (H). The corresponding loss correlation sets predicted the performance of eight impellers as shown in Fig. 7–Fig. 15. The root-mean-square error (RMSE) and maximum error were calculated excluding the error near the choke point.

$$RMSE = \sqrt{\left[(X_{Cal,1} - X_{Exp,1})^2 + (X_{Cal,2} - X_{Exp,2})^2 + \cdots + (X_{Cal,N} - X_{Exp,N})^2\right]/N} \quad (90)$$

where X represents the performance parameters, such as pressure ratio and isentropic efficiency; N represents the amount of samples.

4.2.1. Group 1

Fig. 7 shows the stage total pressure ratio prediction for Impeller (D). The predicted value by Set 1 is more in close to the experimental results compared with that by Oh's set. The RMSE of stage total pressure ratio is about 0.95%. The tendency of the predicted value is consistent with the experimental results in the high mass flow region. The stage total pressure ratio is underestimated near the surge point at all speed lines. A maximum error occurs near the surge point at the speed line of 15000 rpm of about −2.66%.

Fig. 8 shows the stage performance prediction for Impeller (E). Set 1 doesn't function better than Oh's set on stage isentropic efficiency, but slightly outperforms Oh's set on stage total pressure. According to the results of Set 1, the RMSE of stage isentropic efficiency is about 1.22%. The predicted stage isentropic efficiency value is in close agreement with the experimental results in the low mass flow region, but there is substantial deviation in the high mass flow region. The maximum error of the stage isentropic efficiency prediction is about 2.47% at the 6.09 kg/s mass flow point at the 14000 rpm speed line. The predicted stage total pressure ratio value is consistent with the experimental results at low rotational speed lines. The maximum error of about 2.36% occurs in the stage total pressure ratio near the choke point at the 16000 rpm speed line. The RMSE of the overall stage total pressure ratio is about 1.52%.

Fig. 9 shows the stage performance prediction for Impeller (F). Set 1 functions worse than Oh's set on stage isentropic efficiency. The predicted stage isentropic efficiency value deviates considerably from the experimental results. The RMSE of stage isentropic efficiency is about 3.76%. The maximum stage isentropic efficiency error is about 8.01% at the 6.81 kg/s mass flow point at the 16000 rpm speed line, because Set 1 under-predicts choke loss with zero. The RMSE of stage total pressure ratio is about 3.87%. The stage total pressure ratio is under-predicted, especially in the low flow region.

Table 5
Loss distribution comparison under the design condition for Impeller (A) (%).

Correlation No.	Skin friction loss	Blade loading loss	Mixing loss	Clearance loss	Incidence loss	Entrance diffusion loss
1	1.69	1.89	1.68	0.34	6.85	0.31
2	–	0.20	0.008	0.80	1.28	–
3	–	–	–	0.80	0	–
Correlation No.	Choke loss	Shock loss	Disk friction loss	Recirculation loss	Leakage loss	Vaneless loss
1	0	0.36	0.58	1.42	0.90	3.98
2	–	0	2.63	2.92	2.10	–
3	–	–	0.03	–	–	–

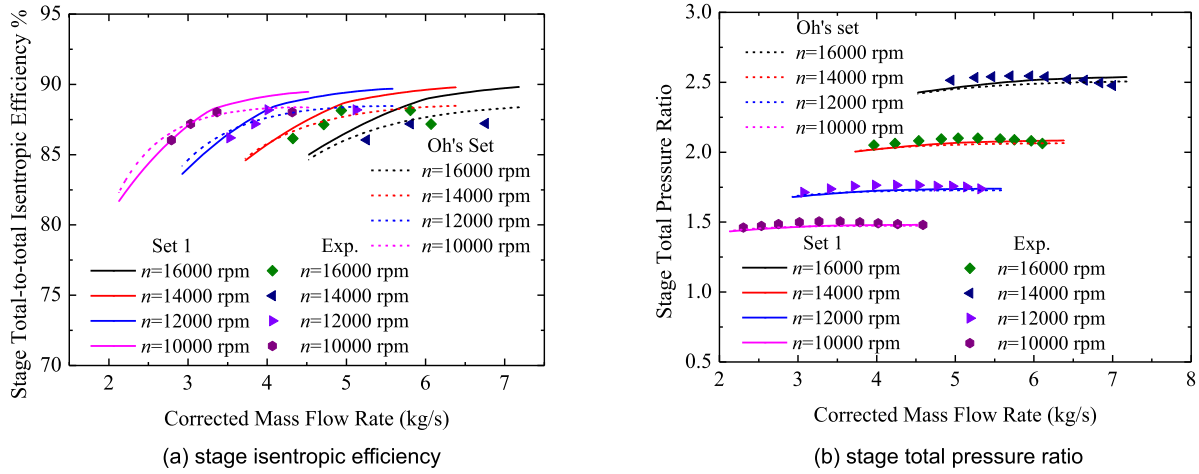

Fig. 8. Stage performance prediction for Impeller (E).

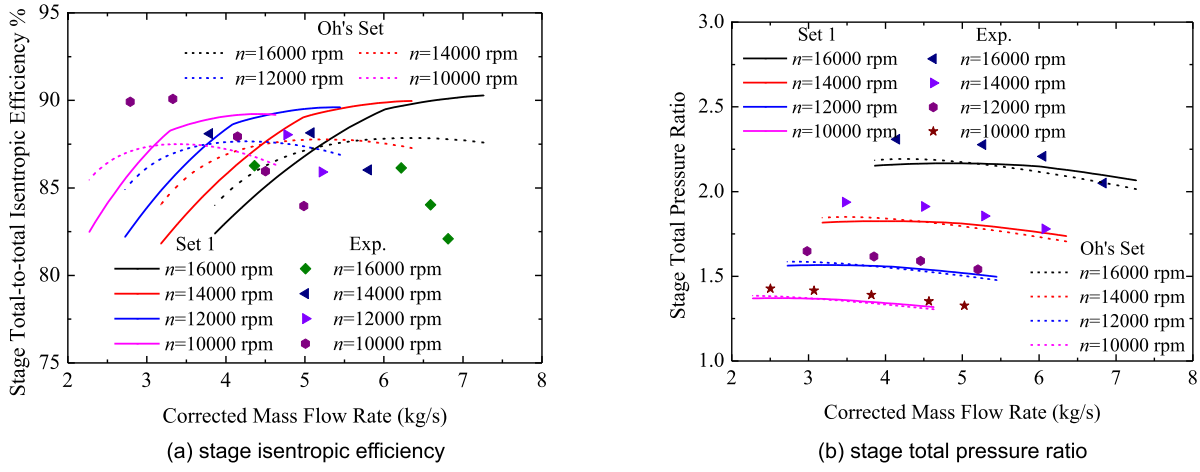

Fig. 9. Stage performance prediction for Impeller (F).

4.2.2. Group 2

Fig. 10 shows the stage performance prediction for Impeller (A). Oh's set greatly under-predicts the stage isentropic efficiency and total pressure ratio. The predicted value by Set 2 is more in close to the experimental results. The RMSE of stage isentropic efficiency is about 2.31%. The predicted efficiency is higher than experimental efficiency under all operation conditions. The maximum stage isentropic efficiency error is about 3.60% near the surge point. The predicted total pressure ratio value is higher than experimental value under all operation conditions and the RMSE of total pressure ratio is about 3.86%.

Fig. 11 shows the impeller performance prediction for Impeller (C). Oh's set greatly underestimates the impeller isentropic efficiency and total pressure ratio. The predicted value by Set 2 is more in close to the experimental results. The RMSE of impeller isentropic efficiency is about 2.53%. The predicted efficiency agrees well with the experimental value at the high speed lines, but there is a great deviation at the low rotational speed line as shown in Fig. 11(a). The maximum error of impeller isentropic efficiency is about −4.78% near the maximum efficiency point at the speed line of 50% n_d. The tendency of the predicted impeller total pressure ratio value is consistent with the experimental results as shown in Fig. 11(b). The RMSE of total pressure ratio is about 3.73%. The total pressure ratio is over-predicted near the choke point.

Fig. 12 shows the stage performance prediction for Impeller (C). Oh's set greatly under-predicts the stage isentropic efficiency and total pressure ratio. The predicted value by Set 2 is more in close

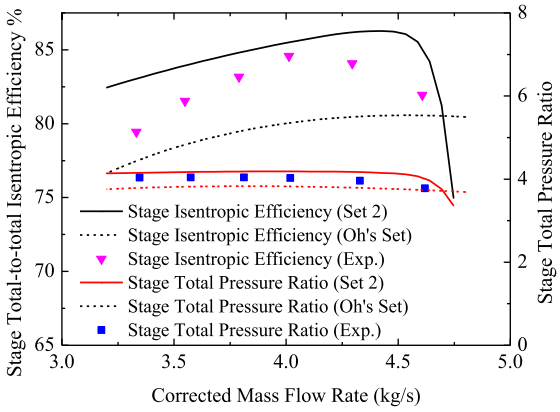

Fig. 10. Stage performance prediction for Impeller (A).

to the experimental results. The RMSE of impeller isentropic efficiency is about 2.70%. The predicted efficiency agrees well with the experimental value at the high speed lines, but there is a great deviation at the low rotational speed line as shown in Fig. 12(a). The maximum error of stage isentropic efficiency is about −4.37% at the speed line of 50% n_d. The predicted stage total pressure ratio values tend to be consistent with the experimental results as shown in Fig. 12(b) and the RMSE of total pressure ratio is about 1.42%. The stage total pressure ratio is over-predicted near the choke point at the speed line of 80% n_d.

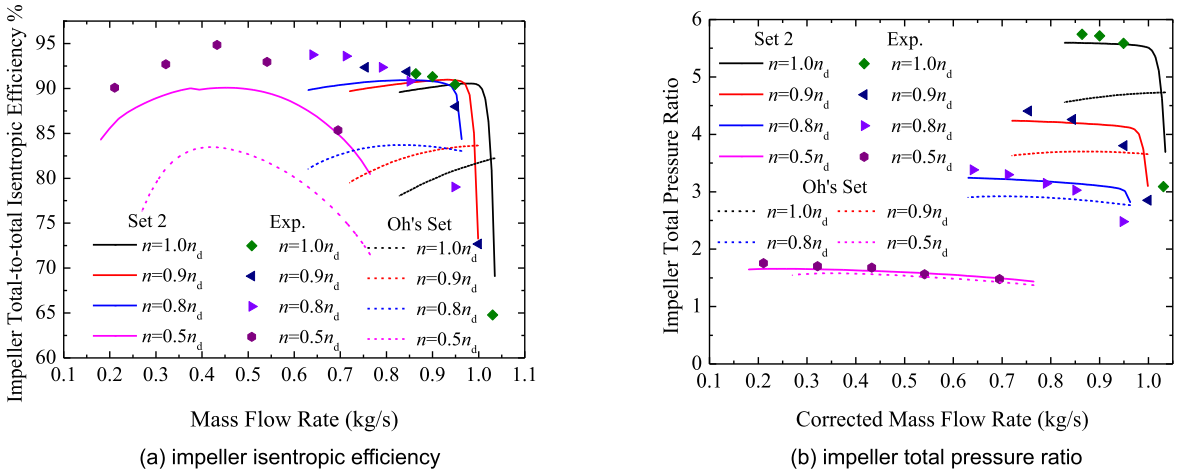

Fig. 11. Impeller performance prediction for Impeller (C).

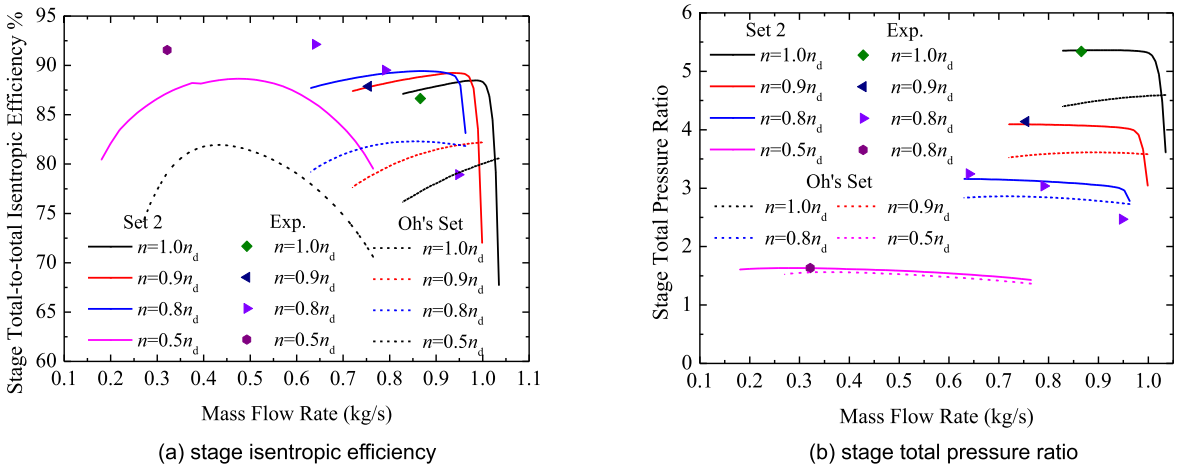

Fig. 12. Stage performance prediction for Impeller (C).

Fig. 13 shows the impeller performance prediction for Impeller (H). Oh's set greatly under-predicts the stage isentropic efficiency and total pressure ratio. The predicted value by Set 2 is more in close to the experimental results. The RMSE of impeller isentropic efficiency is about 1.17%. The impeller isentropic efficiency is low-predicted near the surge point and over-predicted near the choke point. The maximum impeller isentropic efficiency error is about −1.45% near the surge point. The RMSE of impeller total pressure ratio is about 4.16%. The impeller total pressure ratio is over-predicted under all operation conditions.

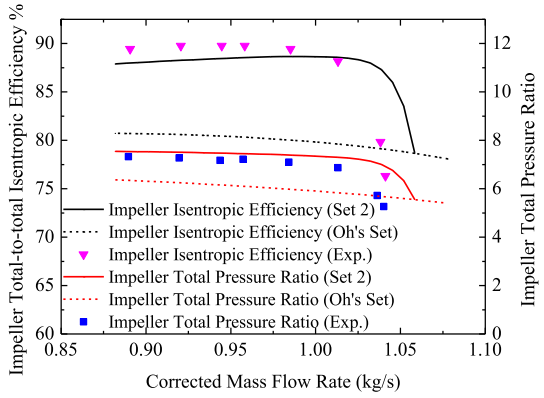

Fig. 13. Impeller performance prediction for Impeller (H).

4.2.3. Group 3

Fig. 14 shows the impeller and stage performance prediction for Impeller (B). Oh's set greatly under-predicts the isentropic efficiency and total pressure ratio. The predicted value by Set 3 is more in close to the experimental results. The RMSE of impeller isentropic efficiency and total pressure ratio is about 1.17% and 7.28%, respectively. The maximum error of impeller isentropic efficiency is about −1.31% near the surge point. The RMSE of stage isentropic efficiency and total pressure ratio is about 0.84% and 7.67%, respectively. The maximum error of stage isentropic efficiency of about 0.36% occurs near the maximum efficiency point. The total pressure ratio is over-predicted near the choke point for both impeller and stage.

The stage performance prediction of Impeller (G) is shown in Fig. 15. Oh's set under-predicts the isentropic efficiency and total pressure ratio greatly in the high flow region but functions well near the surge point. On the whole, the predicted value by Set 3 is more in close to the experimental results. The stage isentropic efficiency and total pressure ratio are both over-predicted under all operation conditions. The RMSE of stage isentropic efficiency and stage total pressure ratio is about 2.46% and 3.92%, respectively. The maximum error of stage isentropic efficiency prediction is about 2.95% near the surge point.

From the results presented above, Oh's set only performs well in lowly-loaded centrifugal compressors but doesn't function well

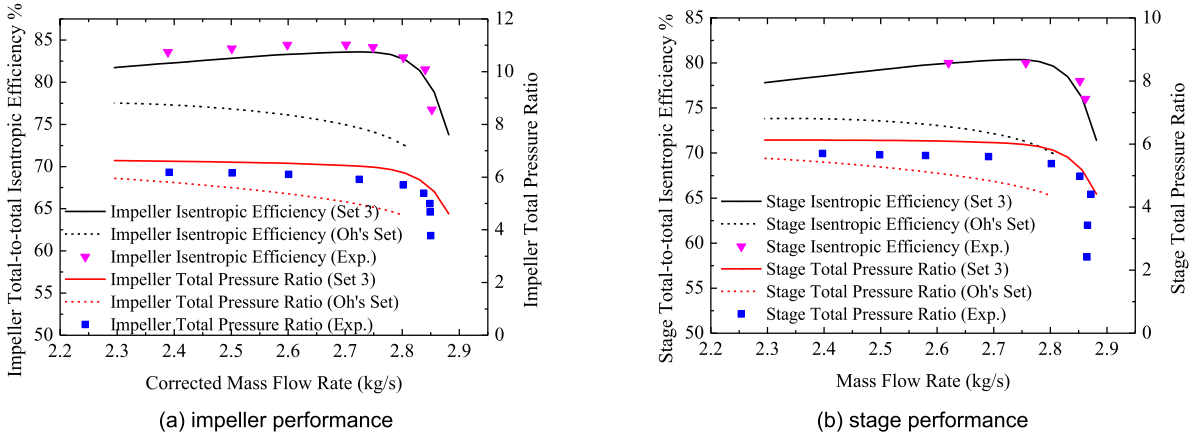

Fig. 14. Performance prediction for Impeller (B).

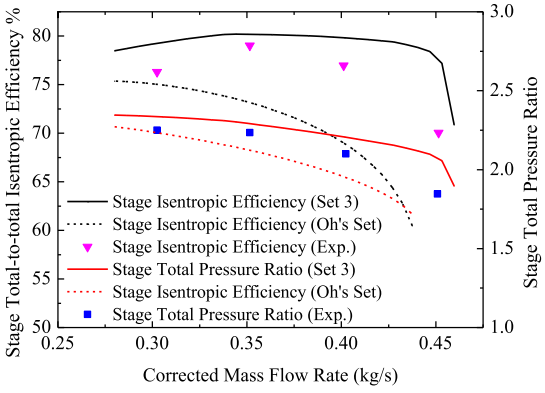

Fig. 15. Stage performance prediction of Impeller (G).

Fig. 16. Test impeller.

Fig. 17. Test rig.

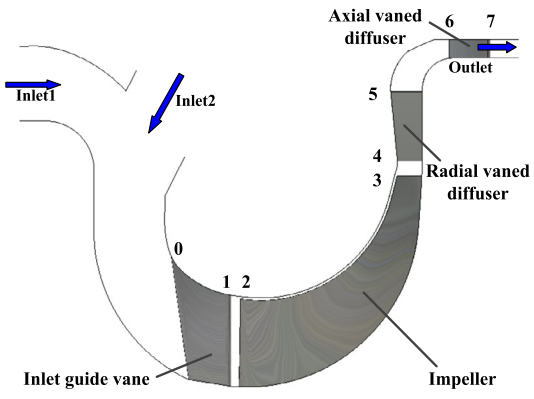

Fig. 18. Flow passage of the centrifugal compressor stage.

in highly-loaded centrifugal compressors. The proposed method outperforms Oh's set, so the hybrid criteria is superior

5. Further validations

The proposed loss correlation selection method is further applied to Impeller (I) for comparison with the experimental results.

5.1. Test facility

Impeller (I) is a backswept impeller with splitter blades as shown in Fig. 16 and Table 6. As shown in Fig. 18, the fluid flows from Inlet 1 and Inlet 2 into the centrifugal compressor stage and mixes fully before flowing into the inlet guide vane. A radial vaned diffuser is attached to the impeller. A passage downstream of the radial diffuser is configured with an axial vaned diffuser. The stage pressure ratio and corrected mass flow rate are 2.67 and 0.45 kg/s at the maximum efficiency point. The stage (Stations 0–7) isentropic efficiency and total pressure ratio are obtained with mass flow at the 100%, 95%, 90% and 75% design speed lines. Fig. 17 shows the centrifugal compressor test rig. The uncertainty of the measured temperature and measured total pressure are within 0.5°C and 0.1%, respectively.

5.2. Results and discussions

The inlet tip relative Mach number (M_{w2t}) is less than 0.8 (Table 6), so the performance of Impeller (I) was evaluated with Set 1. Fig. 19 shows the performance prediction results for Impeller (I) under all operation conditions. Under the design condition,

Table 6
Design parameters of Impeller (I).

Inlet guide vane			
Blade number	19	Exit hub diameter d_{1h}/mm	41.1
Inlet hub diameter d_{0h}/mm	44.4	Exit tip diameter d_{1t}/mm	85.2
Inlet tip diameterd_{0t}/mm	103.6	–	–
Impeller			
Inlet hub diameter d_{2h}/mm	40.9	Mass flow (kg/s)	0.45
Inlet tip diameter d_{2t}/mm	85.6	Rotational speed/rpm	52000
Inlet hub blade angle β_{2h}/deg	43.6	Stage isentropic efficiency/%	79.50
Inlet tip blade angle β_{2t}/deg	60	Stage total pressure ratio	2.67
Exit diameter d_3/mm	143	Tip clearance size/mm	0.2
Exit blade width b_3/mm	6.29	Inlet tip relative Mach no. M_{w2t}	0.65
Exit blade angle β_{3b}/deg	24.5	Specific speed n_s	0.610
Impeller axial length L_z/mm	45.3	Specific diameter d_s	4.142
Exit blade number Z_3	12+12	–	–
Radial vaned diffuser			
Blade number Z_5	21	Exit diameter d_5/mm	183.76
Inlet diameter d_4/mm	150.22	–	–
Axial vaned diffuser			
Blade number Z_7	54	Exit hub diameter d_{7h}/mm	200
Inlet hub diameter d_{6h}/mm	200	Exit tip diameter d_{7t}/mm	208.8
Inlet tip diameter d_{6t}/mm	208.8	–	–

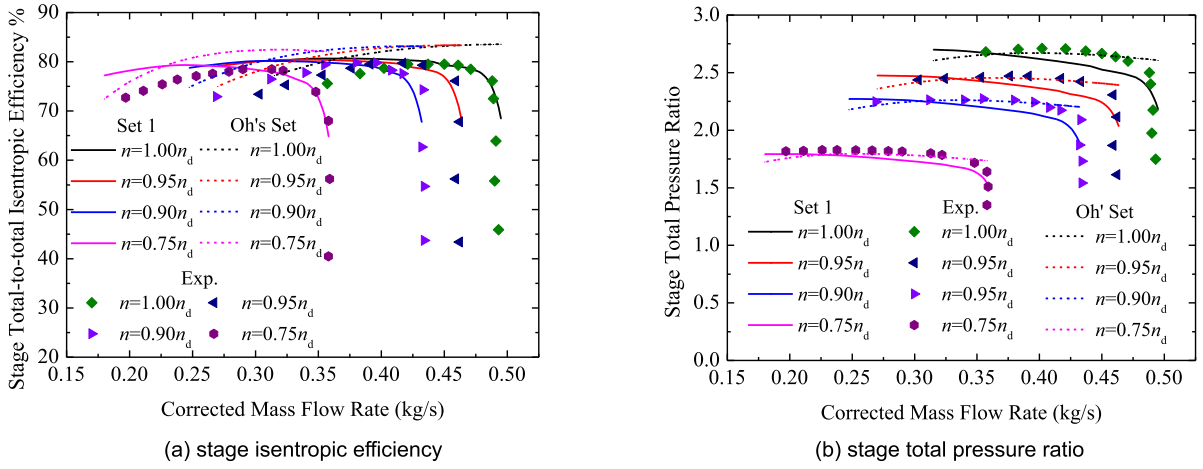

(a) stage isentropic efficiency (b) stage total pressure ratio

Fig. 19. Performance prediction of Impeller (I).

the predicted stage isentropic efficiency is about 79.33%, including 0.07% enthalpy loss in inlet guide vane, 13.06% enthalpy loss in the impeller and 7.54% enthalpy loss in diffuser system. The deviation between the predicted result and experimental result is about −0.17% on the stage isentropic efficiency, while the predicted deviation by Oh's set is about 3.70%. The predicted stage total pressure ratio by Set 1 is about 2.526 and the relative error is about −5.39% compared with the experimental result.

Under the off-design condition, Set 1 outperforms Oh's set on stage isentropic efficiency but does worse than Oh's set on stage total pressure ratio as shown in Fig. 19. For Set 1, the stage isentropic efficiency is predicted well in the high mass flow region but over-estimated in the low mass flow region as shown in Fig. 19(a). The RMSE of stage isentropic efficiency is about 2.91%. The maximum deviation near the surge point at the 75% design speed line is about 6.02%. The predicted stage total pressure ratio values tend to be consistent with the experimental results as shown in Fig. 19(b). The RMSE of stage total pressure ratio is about 3.47%. However, the stage total pressure ratio is underestimated in the low flow region. The maximum error of the stage total pressure ratio prediction is about – 5.38% near the maximum efficiency point at the 100% design speed line.

6. Conclusions

This study was conducted to analyze the loss mechanisms in centrifugal compressors and the corresponding loss correlations. According to the inlet tip relative Mach number (M_{w2t}) and specific speed (n_s), a new method of loss correlations selection was established. The proposed method was validated with experimental results using eight centrifugal compressors in public and one in-house and compared with the conventional loss correlation set.

The main conclusions can be summarized as follows:

- A loss correlation selection method was established according to the inlet tip relative Mach number (M_{w2t}) and specific speed (n_s). When $M_{w2t} < 0.8$, Set 1 is selected; when $M_{w2t} \geq 0.8$ & $n_s < 0.7$, Set 2 is selected; when $M_{w2t} \geq 0.8$ & $n_s \geq 0.7$, Set 3 is selected.
- The performance of eight open-public centrifugal compressors is predicted. The proposed method outperforms the conventional loss correlation set. Under the design condition, the deviations are less than 1.20% on the isentropic efficiency. Under the off-design condition, the RMSE of isentropic efficiency and total pressure ratio are less than 2.53% and 7.67%, respectively, except for Impeller (F).

- The in-house centrifugal compressor performance is evaluated with Set 1. Under the design condition, the deviation between the predicted and experimental results is approximately −0.17% on the stage isentropic efficiency. Under the off-design condition, the RMSE of stage isentropic efficiency and stage total pressure ratio is approximately 2.91% and 3.47%, respectively.
- The proposed method outperforms the conventional set in transonic centrifugal compressors and functions almost as well as the conventional set in subsonic centrifugal compressors.

Declaration of competing interest

The authors declare there is no competing interest.

Acknowledgement

This research was supported by National Key R&D Program of China (2018YFB0905101).

References

[1] M.R. Galvas, Fortran Program for Predicting Off-Design Performance of Centrifugal Compressors, 1973.
[2] O. Conrad, K. Raif, M. Wessels, The calculation of performance maps for centrifugal compressors with vane-island diffusers, in: Performance Prediction of Centrifugal Pumps and Compressors, 1979, pp. 135–147.
[3] A. Whitfield, N.C. Baines, Design of Radial Turbomachines, 1990.
[4] H.W. Oh, E.S. Yoon, M. Chung, An optimum set of loss models for performance prediction of centrifugal compressors, Proc. Inst. Mech. Eng. A, J. Power Energy 211 (1997) 331–338.
[5] J.T. Gravdahl, F. Willems, A.G. de Jager, O. Egeland, Modeling of surge in free-spool centrifugal compressors: experimental validation, J. Propuls. Power 20 (2013) 849–857.
[6] A.A. Doustmohammadi, A. HajilouyBenisi, M. Mojaddam, Experimental and Numerical Investigation of Losses in Centrifugal Compressor Components, 2013, V06CT40A015.
[7] P. Li, C. Gu, Y. Song, A new optimization method for centrifugal compressors based on 1D calculations and analyses, Energies 8 (2015) 4317–4334.
[8] E.I.G. Velásquez, Determination of a suitable set of loss models for centrifugal compressor performance prediction, Chin. J. Aeronaut. 30 (2017) 1644–1650.
[9] P. Thanapandi, R. Prasad, Performance prediction and loss analysis of low specific speed submersible pumps, Proc. Inst. Mech. Eng. A, J. Power Energy 204 (1990) 243–252.
[10] R.H. Aungier, Mean streamline aerodynamic performance analysis of centrifugal compressors, Trans. Am. Soc. Mech. Eng. J. Turbomach. 117 (1995), 360-360.
[11] X. Gong, R. Chen, Total pressure loss mechanism of centrifugal compressors, Mech. Eng. Res. 4 (2014) 45.
[12] M.R. Galvas, Analytical Correlation of Centrifugal Compressor Design Geometry for Maximum Efficiency with Specific Speed, 1972.
[13] W. Jansen, A method for calculating the flow in a centrifugal impeller when entropy gradients are present, in: Royal Society Conference on Internal Aerodynamics (Turbomachinery), 1967, pp. 133–146.
[14] J. Coppage, F. Dallenbach, Study of Supersonic Radial Compressors for Refrigeration and Pressurization Systems, Garrett Corp Los Angeles Ca AiResearch MFG DIV, 1956.
[15] J. Johnston, R. Dean, Losses in vaneless diffusers of centrifugal compressors and pumps: analysis, experiment, and design, J. Eng. Power 88 (1966) 49–60.
[16] C. Rodgers, Paper 5: a cycle analysis technique for small gas turbines, in: Proceedings of the Institution of Mechanical Engineers, Conference Proceedings, Sage Publications, Sage, UK London, England, 1968, pp. 37–49.
[17] Y.A. Spunde, About the Influence of the Clearance Between the Working Blades and Housing of a Radial Turbine on its Exponent, Foreign Technology DIV Wright-Patterson AFB OHIO, 1967.
[18] J.W. Daily, R.E. Nece, Chamber dimension effects on induced flow and frictional resistance of enclosed rotating disks, J. Basic Eng. 82 (1960) 217–230.
[19] D.G. Shepherd, Principles of Turbomachinery, Macmillan, 1956.
[20] M.P. Boyce, Centrifugal Compressors: A Basic Guide, PennWell Books, 2003.
[21] J.D. Stanitz, One-Dimensional Compressible Flow in Vaneless Diffusers of Radial- and Mixed-flow Centrifugal Compressors, Including Effects of Friction, Heat Transfer and Area Change, National Advisory Committee for Aeronautics, 1952.
[22] J.R. Serrano, F.J. Arnau, L.M. Garciacuevas, L.B. Inhestern, An innovative losses model for efficiency map fitting of vaneless and variable vaned radial turbines extrapolating towards extreme off-design conditions, Energy 180 (2019) 626–639.
[23] A. Pinarbasi, Experimental hot-wire measurements in a centrifugal compressor with vaned diffuser, Int. J. Heat Fluid Flow 29 (2008) 1512–1526.
[24] H. Oh, E. Yoon, M. Chung, Systematic two-zone modelling for performance prediction of centrifugal compressors, Proc. Inst. Mech. Eng. A, J. Power Energy 216 (2002) 75–87.
[25] Z. Chao-wei, D. Xue-zhi, L. Xi-yang, G. Qing, T. Chun-qing, An Improved Streamline Curvature Method for Centrifugal Compressor Performance, ASME Paper No. GTINDIA2017-4531, 2017.
[26] A. Zamiri, B.J. Lee, T.C. Jin, Numerical evaluation of transient flow characteristics in a transonic centrifugal compressor with vaned diffuser, Aerosp. Sci. Technol. 70 (2017).
[27] J.D. Stanitz, Effect of Blade-Thickness Taper on Axial-Velocity Distribution at the Leading Edge of an Entrance Rotor-Blade Row with Axial Inlet, and the Influence of this Distribution on Alignment of the Rotor Blade for Zero Angle of Attack, 1953.
[28] H. Kosuge, T. Ito, K. Nakanishi, A consideration concerning stall and surge limitations within centrifugal compressors, J. Eng. Power 104 (1982) 782–787.
[29] C. Yang, W. Wang, H. Zhang, C. Yang, Y. Li, Investigation of stall process flow field in transonic centrifugal compressor with volute, Aerosp. Sci. Technol. 81 (2018) 53–64.
[30] D. Japikse, Advanced diffusion levels in turbocharger compressors and component matching, in: 1st International Conference on Turbocharging and Turbochargers, London, Apr. 1982, pp. 26–28.
[31] R.H. Aungier, Aerodynamic Performance Analysis of Vaned Diffusers, Axial-Flow Compressors, vol. 1, 2003.
[32] R.H. Aungier, Aerodynamic Design and Analysis of Vaneless Diffusers and Return Channels, 1993, V001T003A042.
[33] R.H. Aungier, One-dimensional aerodynamic performance analysis, in: R.H. Aungier (Ed.), Centrifugal Compressors: A Strategy for Aerodynamic Design and Analysis, ASME, New York, NY, 2000.
[34] A. Stodola, Steam and Gas Turbines, P. Smith, 1945.
[35] F. Wiesner, A review of slip factors for centrifugal impellers, J. Eng. Power 89 (1967) 558–566.
[36] X. Qiu, C. Mallikarachchi, M. Anderson, A new slip factor model for axial and radial impellers, in: ASME Turbo Expo 2007: Power for Land, Sea, and Air, American Society of Mechanical Engineers, 2007, pp. 957–966.
[37] C. Zhang, X. Dong, X. Liu, Q. Gao, C. Tan, Improved slip factor model for centrifugal compressor, J. Aerosp. Power 33 (2018) 2178–2187.
[38] J.S. Oh, K.S. Oh, Numerical modeling of some parameters for performance prediction of centrifugal impellers, in: ASME Turbo Expo 2000 Power for Land, Sea, and Air, 2000, V001T003A032.
[39] R.V. Van den Braembussche, Centrifugal Compressors Analysis and Design, Sint-Genesius-Rode, Belgium, 2012.
[40] H. Krain, A CAD method for centrifugal compressor impellers, J. Eng. Gas Turbines Power 106 (1984) 482–488.
[41] H. Krain, Swirling impeller flow, ASME J. Turbomach. 110 (1988) 122–128.
[42] H. Krain, W. Hoffman, Verification of an impeller design by laser measurements and 3D-viscous flow calculations, in: ASME 1989 International Gas Turbine and Aeroengine Congress and Exposition, American Society of Mechanical Engineers, 1989, V001T001A064.
[43] G. Eisenlohr, H. Krain, F.-A. Richter, V. Tiede, Investigations of the Flow Through a High Pressure Ratio Centrifugal Impeller, ASME Paper No. GT2002-30394, 2002.
[44] H. Krain, B. Hoffmann, H. Pak, Aerodynamics of a centrifugal compressor impeller with transonic inlet conditions, in: ASME 1995 International Gas Turbine and Aeroengine Congress and Exposition, American Society of Mechanical Engineers, 1995, V001T001A011.
[45] R. Pampreen, Splitter-Bladed Centrifugal Compressor Impeller Designed for Automotive Gas Turbine Application, 1977.
[46] D. Eckardt, Flow field analysis of radial and backswept centrifugal compressor impellers. I – Flow measurements using a laser velocimeter, in: Performance Prediction of Centrifugal Pumps and Compressors, 1979, pp. 77–86.
[47] S.N. Danish, M. Chaochen, C. Yang, The influence of tip clearance on centrifugal compressor stage of a turbocharger, in: Proceedings of 4th IASME/WSEAS Int. Conf. on Fluid Mechanics and Aerodynamics, Elounda, Agios Nikolaos, Crete Island, Greece, 2006.
[48] J.S. Oh, S.H. Ro, Analysis of 8 Centrifugal Compressor Impellers Using Two Different CFD Methods: Part I — Code Validation, 2001.
[49] G. Perrone, M. Holbrook, J. McVaugh, Backswept Impeller and Vane Island Diffuser and Shroud for NASA Advanced-Concepts Compressor Test Rig, 1973.
[50] Z. Wang, B. Lu, J. Liu, J. Hu, Numerical simulation of unsteady tip clearance flow in a transonic compressor rotor, Aerosp. Sci. Technol. 72 (2018) 193–203.
[51] M. Kaneko, H. Tsujita, Influences of Tip Leakage Flows Discharged From Main and Splitter Blades on Flow Field in Transonic Centrifugal Compressor Stage, 2018, V02BT44A006.
[52] M. Casey, C. Robinson, C. Zwyssig, The Cordier Line for Mixed Flow Compressors, ASME Paper No. GT2010-22549, 2010.